THz-Time Domain Spectroscopy and IR on MoS_2

David Arcos[1], Daniel Gabriel[1], Dumitru Dumcenco[2], Andras Kis[2], Núria Ferrer-Anglada[*,1]

[1] Applied Physics Department, Universitat Politècnica de Catalunya (UPC), Campus Nord B4, J. Girona 3-5, 08034 Barcelona, Spain
[2] Electrical Engineering Institute, École Polytechnique Féderale de Lausanne (EPFL), Lausanne, Switzerland[1]

Received ZZZ, revised ZZZ, accepted ZZZ
Published online ZZZ (Dates will be provided by the publisher.)

Keywords MoS_2, graphene, IR spectroscopy, high frequency conductivity, THz-time domain spectroscopy, transmittance.

* Corresponding author: e-mail nuria.ferrer@upc.edu, Phone: +34 934 016 880, Fax: +34 934 016 090

In the increasing research field of 2D materials such graphene, molybdenum disulfide MoS_2 attracted a great interest due to the existence of a direct bandgap in monolayer MoS_2, which gives the possibility of performing MoS_2 field-effect transistors or optoelectronic devices. We analyzed by THz-Time Domain Spectroscopy (THz-TDS) up to 2 THz and infrared (IR) spectroscopy, CVD obtained MoS_2 using either S or H_2S gas as a sulfur precursor, grown on a sapphire substrate. From THz-TDS we obtained the transmittance, conductivity and attenuation. From IR spectroscopy on the same samples we deduced the transmittance at IR frequency range. We observed the coherence of both spectroscopic methods. The advantage of THz-TDS method is that we can get significant parameters related to the sample quality without the need of depositing any electrical contact or sample preparation. Our results show that at high frequencies MoS_2 is even better than graphene as a material for optoelectronic devices.

1 Introduction Recent advances in fabrication of ultrathin layered materials down to atomic thickness have contributed towards the exploration of new low-dimensional physics.

Transition metal dichalcogenides have attracted considerable attention due to their potential applications as new materials in the fields of catalysis, nanotribology, microelectronics, lithium batteries, medical and optoelectronics [1, 2] with applications as thin film transistors, light-emitting diodes [3] or photodetectors [4]. In particular, molybdenum disulfide (MoS_2) is a two-dimensional material that recently has attracted increasing attention. In the bulk MoS_2 crystal, S-Mo-S layers are Van der Waals bonded [5], each of these layers (MoS_2 monolayer) can be considered as two hexagonal planes of S atoms and an intermediate hexagonal plane of Mo atoms bonded by covalent interactions with the S atoms in a trigonal prismatic structure (Fig. 1).

It is well known that bulk MoS_2 has an indirect band gap of 1,29 eV, whereas the monolayer MoS_2 shows a direct band gap of 1,80 eV.

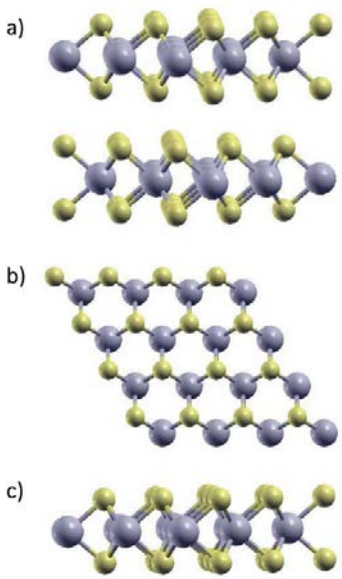

Figure 1 a) Side view of bulk MoS_2. b) Top view of bulk and monolayer MoS_2, Mo atoms are presented by spheres bigger than S. So for bulk MoS_2, the Mo atoms of 2nd layer must be seen. c) - Side view of monolayer MoS_2. The Mo-atoms are depicted by gray and S-atoms by yellow [6].

Terahertz (THz) spectroscopy and imaging provides a powerful tool for the characterization of different kind of materials, including semiconductors. In the last few years

there has been an increasing interest in terahertz imaging and spectroscopy for optoelectronic applications, and more and more terahertz characterization are being reported [7, 8].

The infrared spectroscopy (IR) analysis is important for its role in optoelectronic implementations. Both graphene and MoS_2 characterization on the THz and IR bands are a key requirement for its applications and development on optoelectronic devices.

2 Sample preparation and characterization We analyzed an overall of 4 samples of pristine graphene transferred on a polyethylene terephthalate (PET) substrate and 4 samples of MoS_2 grown on sapphire substrates.

Table 1 Summary of samples S_i, graphene or MoS_2 and their substrate, analyzed in the current study. Sample identification are used for later reference.

Substrate	Material	Sample	Growth	Number of samples
PET	Graphene	S_1	CVD	4
Sapphire	MoS_2	S_2	CVD-S	2
Sapphire	MoS_2	S_3	CVD-H_2S	2

Graphene are obtained by chemical vapor deposition (CVD) transferred on a PET substrate and MoS_2 are obtained by CVD-S and CVD-H_2S, table 1, described briefly in the next section. Samples S_1 are obtained at Sejong University as described in [9], and S_2 and S_3 are from the École Polytechnique Féderale de Lausanne (EPFL) as described in [10].

Structural quality, homogeneity and domain size are described in ref [10] for MoS_2, and in ref [11] for graphene. Domain size is from 5 to 10 µm for MoS_2, and from 1 to 5 µm for graphene. Structural quality is tested by Raman, that shows good quality with low amount of defects.

2.1 CVD-S MoS_2 and CVD-H_2S MoS_2 Chemical vapor deposition (CVD) is the most promising method to synthesize monolayer materials. In particular, MoS_2 can be obtained from triangular islands up to a large-scale film, depending on the growing conditions.

For sample CVD-S we used the commonly CVD method, which involves a solid sulfur source plus an inert gas (Ar) as a carrier gas flow. For CVD-H_2S we used a gas-phase precursor, a mixture H_2S:H_2 at different conditions of temperature and mixture ratio. Selecting both conditions allow us to regulate the growth direction: when the injected gas temperature is 600ºC or lower and the ratio H_2S:H_2 = 3:1, the growing is horizontal and a centimeter-scale MoS_2 monolayer is obtained, showing a morphology based on triangular shape domains that merge in a continuous film [10].

2.2 Raman characterization Raman spectroscopy is performed with an excitation laser of 532 nm, with a pin hole size of 150 µm, 100x objective, and a power of 0.5 mW that ensures the non-degradation of the sample. A quick and accurate sample identification (Fig. 2) are given by the Raman spectra.

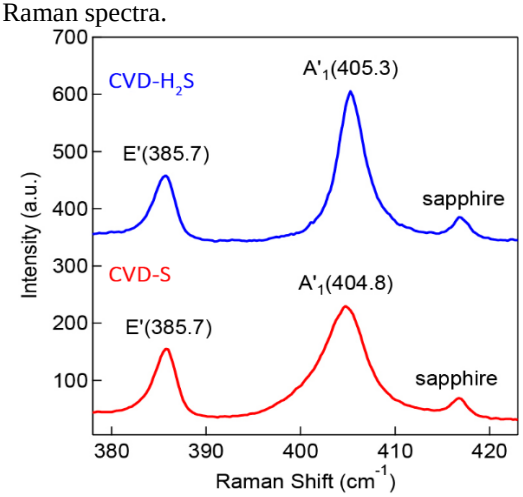

Figure 2 (Color online) From top to bottom, Raman spectra of CVD-H_2S MoS_2, S_3, and CVD-S MoS_2, S_2, on sapphire substrate.

Like graphene, single-layer and few-layer MoS_2 has distinctive signatures in its Raman spectrum. The Raman spectrum of bulk MoS_2 has two prominent peaks: an in-plane mode (E_{2g}^1 or E' on Fig. 2) located around 383 cm^{-1} and an out-of-plane mode (A_{1g} or A'$_1$ on Fig. 2) which is located at 408 cm^{-1}. The E_{2g}^1 line corresponds to the sulfur atoms vibrating in one direction and the molybdenum atom in the other, while the A_{1g} line corresponds to just the sulfur atoms vibrating out-of-plane. As MoS_2 becomes single-layer, the in-plane and out-of-plane modes, E_{2g}^1 and A_{1g}, evolve with thickness. The in-plane mode upshifts to 385 cm^{-1} and the out-of-plane downshifts to 403 cm^{-1} [12].

Both CVD-S and CVD-H_2S MoS_2 present similar Raman spectra but with some important differences. Both materials present an E_{2g}^1 line located at 385.7 cm^{-1}, while the out-of-plane vibration, A_{1g}, are located at different frequencies, at 404.8 cm^{-1} (for sample CVD-S) and 405.3 cm^{-1} (for CVD-H_2S). The difference between A_{1g} and E_{2g}^1 modes for both samples are ~20 cm^{-1}, therefore, we can assume that both MoS_2 are monolayers [12].The softening and broadening of the out-of-plane A_{1g} mode could be explained by different doping levels of MoS_2, increasing the doping level causes broadening on the A_{1g} mode and decreases the intensity ratio between A_{1g} and E_{2g}^1 modes, indicating in our case a greater doping level for sample CVD-S [13].

The different A_{1g} mode position in Raman spectra between presented CVD-S and previous results corresponds to slightly different grown conditions of MoS_2 [14].

Raman spectra were taken using different sample zones, from 5 to 10 different points. In most of them the spectra are similar.

3 Experimental

3.1 THz-Time Domain Spectroscopy Terahertz time-domain spectroscopy (THz-TDS) is a contactless, non-destructive spectroscopic technique based on a coherent detection scheme. Material complex properties can be measured at THz frequencies, up to 2 THz, by using a phase-sensitive technique. The THz measurements are collected using a THz-TDS spectrometer in transmission setup, based on the commercial TERA K8, from Menlo Systems (Fig. 3).

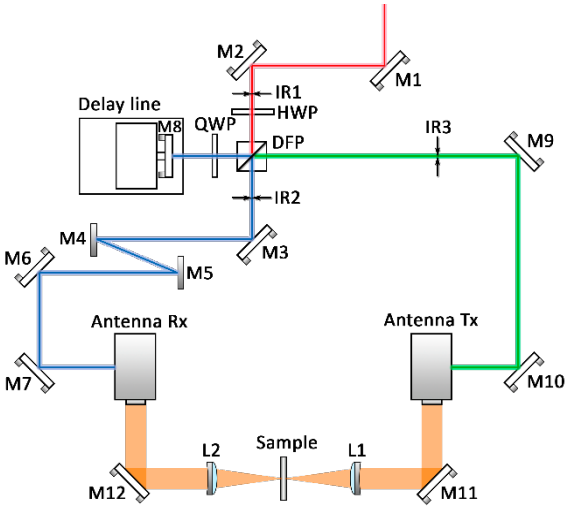

Figure 3 THz-TDS transmission setup configuration.

Broadband THz radiation is generated by using a 780 nm wavelength fs laser and is later detected with a photoconductive antenna. The output of the laser is split into a pump (generating) and a probe (detecting) beams using a polarizing beam splitter, where each of these beams travel through two different optical paths to the emitter and the detector antenna, respectively.

The probe (detecting) path implements a variable length using a delay line, to control the pulses delay arriving to the receiver antenna.

The pump (generating) beam is collimated to the emitter antenna with the purpose to produce a THz electric field that is transmitted through the sample and is modified by its frequency response. The beam spot size at the sample surface is about 550 µm, after the Menlo Systems specifications, but it could be slightly larger, close to 1 mm, when working. The modified electric field is focused on a THz detector photoconductive antenna, which is gated by the probe (detection) laser beam. As a result, a time-domain electric field pulse is obtained. The recorded time-domain trace is transformed into the frequency domain by using the Fourier transform (FFT) for spectroscopic analysis. From the frequency spectra, the refractive index, the conductance and attenuation of the sample can be deduced.

3.2 THz-TDS experimental results

We analyze, using the THz time-domain spectroscopy, the conductivity of different MoS_2 samples grown on sapphire and, just for comparison, CVD obtained graphene [11] transferred on a PET substrate at high frequencies, from 100 GHz to 2 THz.

From the time-domain electric field, see Fig. 4, provided by the THz-TDS spectroscopic method, we obtain its THz spectrum, see Fig. 5, by applying the FFT on the time signal. Hence, we obtain information of both the amplitude and the phase of the THz waves in frequency domain.

By analyzing the time domain electric field (Fig. 4), we observe that a monolayer MoS_2 on sapphire substrate causes a 5.68% decrement at the maximum value of the temporal pulse, as we see in the inset.

Since water has a strong absorption in many of the frequency bands in the THz range, high relative humidity of the environment would therefore greatly affect the frequency spectra at certain frequencies. The water absorption of the THz wave causes an absorption peak in the frequency spectra of the measured temporal electric field (Fig. 5).

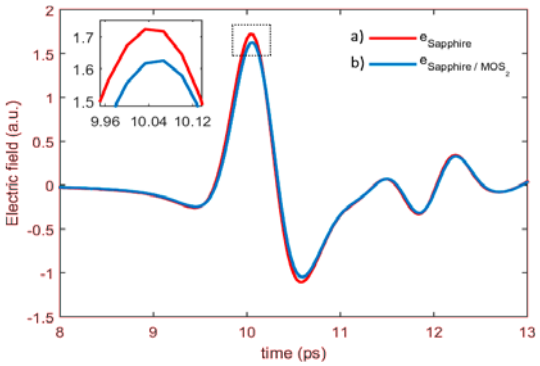

Figure 4 (Color online) Time-domain electric field pulse of the transmitted THz wave through a) the bare sapphire substrate and b) the MoS_2 grown on a sapphire surface, corresponding to sample S_2.

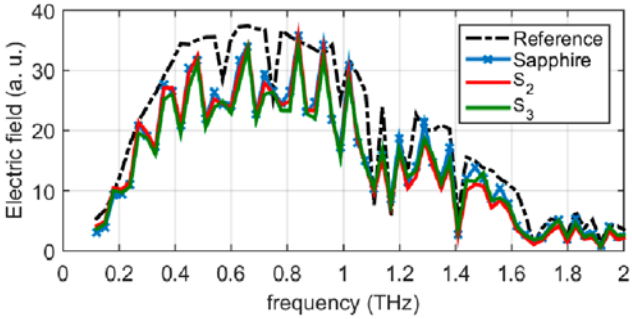

Figure 5 (Color online) Frequency spectrum of the measured temporal electric field pulse of the transmitted THz wave through

the reference (air), the bare substrate (sapphire) and the MoS_2 grown on a sapphire surface, corresponding to samples S_2 and S_3.

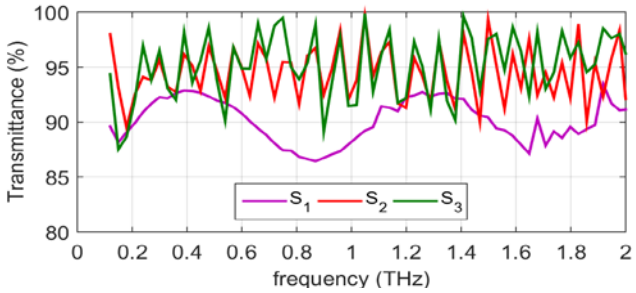

Figure 6 (Color online) MoS_2 and graphene transmittance. On the left, from top to bottom: (S_2) CVD-S MoS_2 on sapphire, (S_3) CVD-H_2S MoS_2 on sapphire and (S_1) CVD graphene on PET.

Transmittance represents the intensity portion of the THz wave transmitted through a material and air is used as the transmission reference. Hence, transmittance is defined as the ratio between the frequency domain wave transmitted through the sample and the reference wave, as follows:

$$T(\omega) = \frac{FFT[e(t)]}{FFT[e(t)_{reference}]} \quad (1)$$

MoS_2 and graphene transmittance (Fig. 6) are retrieved by using the ratio of the sample (material and substrate) and the bare substrate transmittance:

$$T(\omega)_{material} = \frac{T(\omega)_{material+substrate}}{T(\omega)_{substrate}} \quad (2)$$

The internal Fabry-Pérot reflections, related to the substrate thickness, cause a set of the oscillations seen on Fig. 6.

Graphene (S_1) transmittance in the THz ranges from 87% to 93% approximately, whereas CVD-S and CVD-H_2S MoS_2 (S_2 and S_3 respectively) show a transmittance close to 95%.

Using the transmittance of the sample and the bare substrate, we are able to determine a large set of optoelectronic properties, such as the complex refractive index (Fig. 7), the sheet conductivity of graphene and MoS_2 (Fig. 8), and their attenuation (Fig. 9), among others [11, 15].

First, we characterize the complex refractive indices, see Fig. 7, of the PET and sapphire substrates, by comparing the substrate signal spectrum with the reference (air) spectrum, whereas we minimize the internal Fabry-Pérot reflection effects produced in thin films [15]. With the complex refractive index, we are able to characterize the substrate and then, we can evaluate the sheet conductivity of MoS_2 and graphene [15].

We found that by growing MoS_2 or transferring graphene on to the bare substrate surface, see Fig. 7a, has no bearing on the values of the sample refractive index.

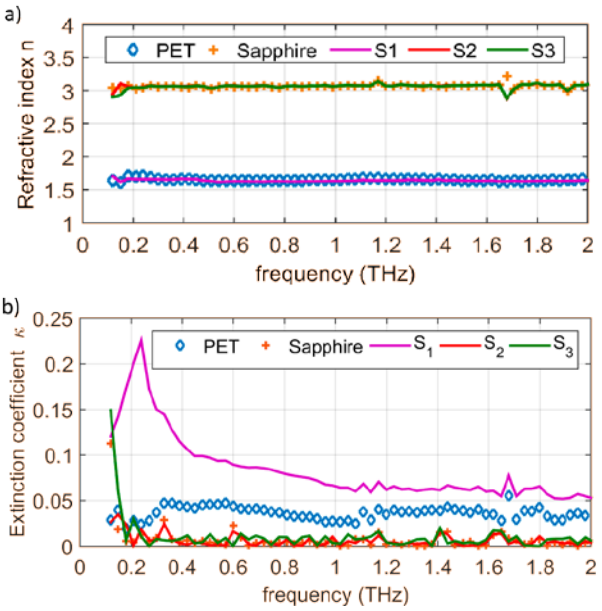

Figure 7 (Color online) a) Real part of the refractive indices and b) Imaginary part of the refractive indices of substrates, and the samples composed of the material grown on to the substrate surface. On the left, from top to bottom, Sapphire, (S_2) CVD-S MoS_2 on sapphire, (S_3) CVD-H_2S MoS_2 on sapphire, graphene on PET (S_1) and PET.

We deduced the sheet conductivity of MoS_2 and graphene deposited on their respective substrates. To obtain the MoS_2 and graphene conductivity, we have treated them as boundary condition with finite sheet conductivity [15]:

$$T(\omega) = \frac{4\chi \cdot n_{sub}}{n_{sub}+1}\exp(-j(n_{sub}-1)k_0 d_{sub}) \cdot \sum_{FP=0}^{N}\left(\exp(-2jn_{sub}k_0 d_{sub})\frac{n_{sub}-1}{n_{sub}+1}(2n_{sub}\chi - 1)\right)^{FP} \quad (3)$$

Where $\chi^{-1} = 1 + n_{sub} + \sigma_s Z_0$; n_{sub} and d_{sub} are the substrate complex refractive index and thickness, respectively; k_0 is the free-space wave number, Z_0 is the free-space impedance, σ_s is the surface conductivity of the thin film, and FP corresponds to the internal Fabry-Pérot reflections. As the sample thickness is about a hundred µm, we can consider that infinite internal reflections occur in a thin layer, and (Eq. (3)) can be simplified:

$$T(\omega) = \frac{4\chi \cdot n_{sub}}{n_{sub}+1}\exp(-j(n_{sub}-1)k_0 d_{sub}) \cdot \frac{1}{1-\exp(-2jn_{sub}k_0 d_{sub})\frac{n_{sub}-1}{n_{sub}+1}(2n_{sub}\chi - 1)} \quad (4)$$

Table 2 Real part of refractive indices of the substrates, sheet conductivity's smooth values and normalized sheet conductivity of the material σ_s (in mS) and normalized sheet conductivity's smooth values σ_n of the material at 1 THz, 1.5 THz and 2 THz, normalized to the conductance quantum, G_0.

Substrate	Sample	Growth	Material	n	σ_n (1 THz)	σ_s (1 THz)	σ_n (1.5 THz)	σ_s (1.5 THz)	σ_n (2 THz)	σ_s (2 THz)
PET	S_1	CVD	Graphene	1.65	15.28	1.18	25.98	2.01	20.89	1.62
Sapphire	S_2	CVD-S	MoS_2	3.07	13.93	1.08	29.59	2.29	47.95	3.72
Sapphire	S_3	CVD-H_2S	MoS_2	3.07	32.89	2.55	75.14	5.82	109.39	8.48

Finally, with all the parameters known, we can extract the MoS_2 and graphene conductivity, see Fig. 8, reported on the right by its normalized conductance quantum units, denoted by the symbol G_0, defined as the quantum unit of electrical conductance:

$$G_0 = \frac{2e^2}{h} \approx 77.48\ \mu S \tag{5}$$

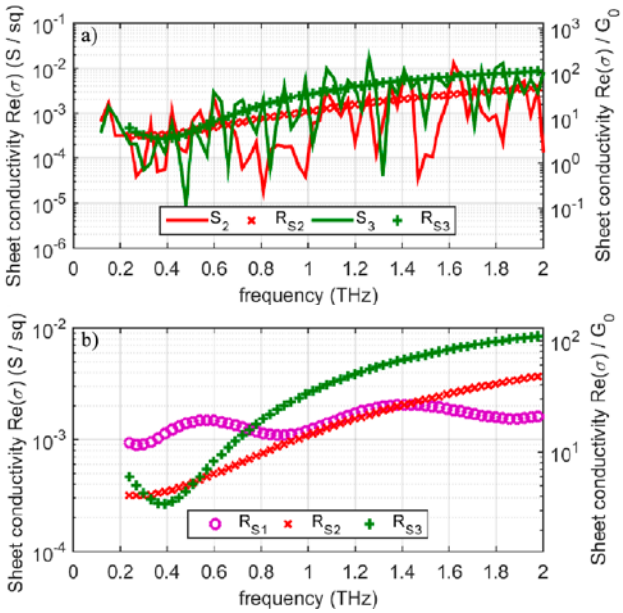

Figure 8 (Color online) Real part of sheet conductivity of MoS_2 and graphene. a) Sheet conductivity of: CVD-S MoS_2, S_2, and CVD-H_2S MoS_2, S_3. RS_2 and RS_3 are a graphical representation of the smooth curve that shows the tendency of the sheet conductivity of CVD-S an CVD-H_2S MoS_2, respectively. b) On the left, from top to bottom: smooth curve of real part of sheet conductivity of (S_1) CVD graphene on PET, (S_3) CVD-H_2S MoS_2 on sapphire and (S_2) CVD-S MoS_2 on sapphire.

As seen in Fig. 8, CVD pristine graphene presents a sheet conductivity around 12-25× the value of quantum conductance, G_0, at frequencies of THz, as expected from previous studies [16, 17]. MoS_2, on the other hand, has a slight difference in values depending on the growth conditions. CVD-S MoS_2, S_2, shows a sheet conductivity around 4.5-42× the value of G_0 whereas CVD-H_2S MoS_2, S_3, presents values 1.3-3 times greater than CVD-S, in the range from 3.4-130× the value of G_0.

By comparing graphene and MoS_2, we observed some different results depending on the frequency range. Specifically, at frequencies below to 750 GHz, graphene sheet conductivity is feebly higher than both CVD-S and CVD-H_2S MoS_2. From 1 to 1.5 THz, CVD-S MoS_2 sheet conductivity is similar to graphene. Finally, at frequencies greater than 1.5 THz, both CVD-S and CVD-H_2S MoS_2 sheet conductivities are slightly higher, up to 3 times, than graphene.

We obtained the attenuation of both MoS_2 and graphene. Attenuation is defined as the intensity loss wave propagation, as follows:

$$A(\omega) = 20\log_{10}(|T(\omega)|) \tag{6}$$

Attenuation of graphene and MoS_2 are illustrated on Fig. 9. We found that CVD pristine graphene, S_1, presents an attenuation from 0.6 to 1.2 dB, whereas MoS_2, shows an attenuation below than 1.8 dB, in detail, CVD-S MoS_2 attenuation, S_2, takes values from 0.1 to 1.7 dB and CVD-H_2S MoS_2, S_3, from 0.1 to 1.8 dB.

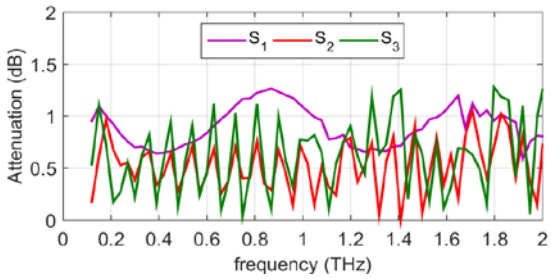

Figure 9 (Color online) Attenuation of MoS_2 and graphene. On the left, from top to bottom: (S_1) CVD graphene on PET, (S_3) CVD-H_2S MoS_2 on sapphire and (S_2) CVD-S MoS_2 on sapphire.

3.3 Infrared spectroscopy We studied MoS_2 transmittance in the infrared band, see Fig. 10, in the range from 400 cm^{-1} to 8000 cm^{-1}. Graphene IR spectroscopy is reported on reference [11]. Measures have been collected with the Frontier FT-IR/FIR Spectrometer from Perkin Elmer at CCiTUB.

It is important to emphasize that, as the MoS_2 transmittance is extracted by comparison (Eq. (2)) using substrate transmittance, we can only determine the material transmittance as long as the transmittance of both the sample and the bare substrate are not null. Therefore, because the sapphire transmittance is null at wavenumber below to

1700 cm^{-1}, we can only study the transmittance of MoS_2 in the range from 1700 cm^{-1} to 8000 cm^{-1}, where MoS_2 present values of transmittance close to 99.8%, see Fig. 10.

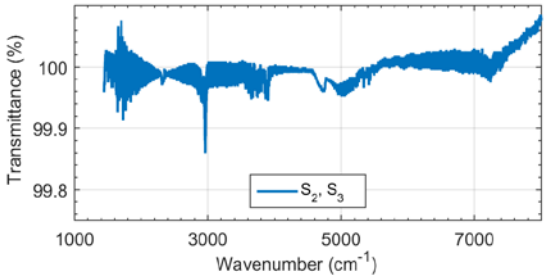

Figure 10 (Color online) IR transmittance of MoS_2.

4 Discussion and conclusions We have characterized electronic properties of CVD MoS_2 and graphene over the THz and IR range.

We studied electronic properties of CVD monolayers of MoS_2 depending on the growth conditions, by controlling the growth direction of MoS_2 domains using H_2S as a gas-phase precursor (CVD-H_2S), in addition to conventional sulfur (CVD-S).

We found that CVD-S MoS_2 presents a sheet conductivity of 4.5-42× the value of quantum conductance, G_0, whereas CVD-H_2S MoS_2 presents values in the range from 3.4-130× the value of G_0, while graphene shows a sheet conductivity around 12-25× the value of G_0. Therefore, we found that CVD monolayer MoS_2 sheet conductivity, at frequencies in the range 1 – 2 THz, is up to 3 times greater for MoS_2 obtained using H_2S as a sulfur gas precursor than the usual CVD MoS_2 obtained with sulfur. Probably, because the former is more ordered.

The attenuation on differently obtained MoS_2 in the THz range are presented, and for comparison, also the graphene attenuation. We observed that monolayer MoS_2 shows an attenuation below than 1.8 dB. In comparison, graphene presents an attenuation from 0.6 to 1.2 dB, similar to MoS_2.

The study of a material transmittance is a key factor to characterize a material over a wide frequency range. We found that at THz frequencies, from 100 GHz to 2 THz, CVD-S and CVD-H_2S MoS_2 transmittance is close to 95%, similar to graphene. On the other hand, at IR wavenumbers, CVD-S an CVD-H_2S MoS_2 transmittance is close to 99.8%. Therefore, the use of MoS_2 is very promising in the development of optoelectronic devices, with similar properties than graphene. Moreover, the existing gap in MoS_2 will provide the possibility to perform transistors for flexible or transparent electronics.

Acknowledgements The authors thank the CCiTUB services for Raman, IR and the AntennaLAB group from Dept. of Signal Theory and Communications of UPC. D. Dumcenco and A. Kis work was financially supported by funding from the Swiss SNF Sinergia Grant no. 147607. D. Dumcenco work was carried out in frames of the Marie Curie ITN network "MoWSeS" (grant no. 317451). We acknowledge partially funding by the EC under the Graphene Flagship (grant agreement no. 604391).

References

[1] Y. Lee, X. Zhang, W. Zhang, M. Chang, C. Lin, K. Chang, Y. Yu, J. T. Wang, C. Chang and L. Y. L. T. Li, *Adv. Mater.*, vol. 24, no. 17, pp. 2320-2325, 2012.

[2] W. Zhu, T. Low, Y. Lee, H. Wang, D. B. Farmer, J. Kong, F. Xia and P. Avouris, *Nature Communications*, vol. 5, p. 3087, 2014.

[3] B. Radisavljevic, A. Radenovic, J. Brivio, V. Giacometti and A. Kis, *Nature Nanotech*, vol. 6, no. 3, pp. 147-150, 2011.

[4] O. Lopez-Sanchez, D. Lembke, M. Kayci, A. Radenovic and A. Kis, *Nature Nanotech*, vol. 8, no. 7, pp. 497-501, 2013.

[5] K. F. Mak, C. Lee, J. Hone and J. Y. H. T. F. Shan, *Phys. Rev. Lett.*, vol. 105, no. 13, p. 136805, 2010.

[6] S. Ahmad and S. Mukherjee, *Graphene*, vol. 3, no. 4, pp. 52-59, 2014.

[7] M. Tonouchi, *Nature Photonics*, vol. 1, no. 2, pp. 97-105, 2007.

[8] X. Zhang and J. Xu, New York: Springer, 2010.

[9] M. F. Khan, M. Z. Iqbal, M. W. Iqbal, V. M. Iermolenko, H. M. Waseem Khalil, J. Nam, K. S. Kim, H. Noh and J. Eom, *RSC Adv.*, vol. 5, no. 62, pp. 50040-50046, 2015.

[10] D. Dumcenco, D. Ovchinnikov, O. Lopez Sanchez, P. Gillet, D. T. L. Alexander, S. Lazar, A. Radenovic and A. Kis, *2D Mater.*, vol. 2, no. 4, p. 044005, 2015.

[11] D. Gabriel, B. Sempere, C. Colominas and N. Ferrer-anglada, *Phys. Status Solidi B*, vol. 252, no. 11, pp. 2423-2428, 2015.

[12] H. Li, Q. Zhang, C. C. R. Yap, B. K. Tay, T. H. T. Edwin, A. Olivier and D. Baillargeat, *Adv. Funct. Mater.*, vol. 22, no. 7, pp. 1385-1390, 2012.

[13] B. Chakraborty, A. Bera, D. V. S. Muthu, S. Bhowmick, U. V. Waghmare and A. K. Sood, *Phys. Rev. B*, vol. 85, no. 16, p. 161403, 2012.

[14] D. Dumcenco, D. Ovchinnikov, K. Marinov, P. Lazić, M. Gibertini, N. Marzari, O. L. Sanchez, Y. Kung, D. Krasnozhon, M. Chen, S. Bertolazzi, P. Gillet, A. Fontcuberta I Morral, A. Radenovic and A. Kis, *ACS Nano*, vol. 9, no. 4, pp. 4611-4620, 2015.

[15] M. Liang, M. Tuo and H. Xin, "Terahertz Characterization of Carbon Nanotube and Graphene On-Substrate Thin Films," in *7th European Conference on Antennas and Propagation (EuCAP)*, Gotenburg, 2013.

[16] W. Liu, R. V. Aguilar, Y. Hao, R. S. Ruoff and N. P. Armitage, *J. Appl. Phys.*, vol. 110, no. 8, p. 083510, 2011.

[17] N. Rouhi, D. Jain, S. Capdevila, L. Jofre, E. Brown and P. J. Burke, *2011 11th IEEE International Conference on Nanotechnology*, 2011.